Appendix

1. Appendix figures

2. Appendix figures legends

3. Appendix methods

4. Appendix results

Appendix figure S1

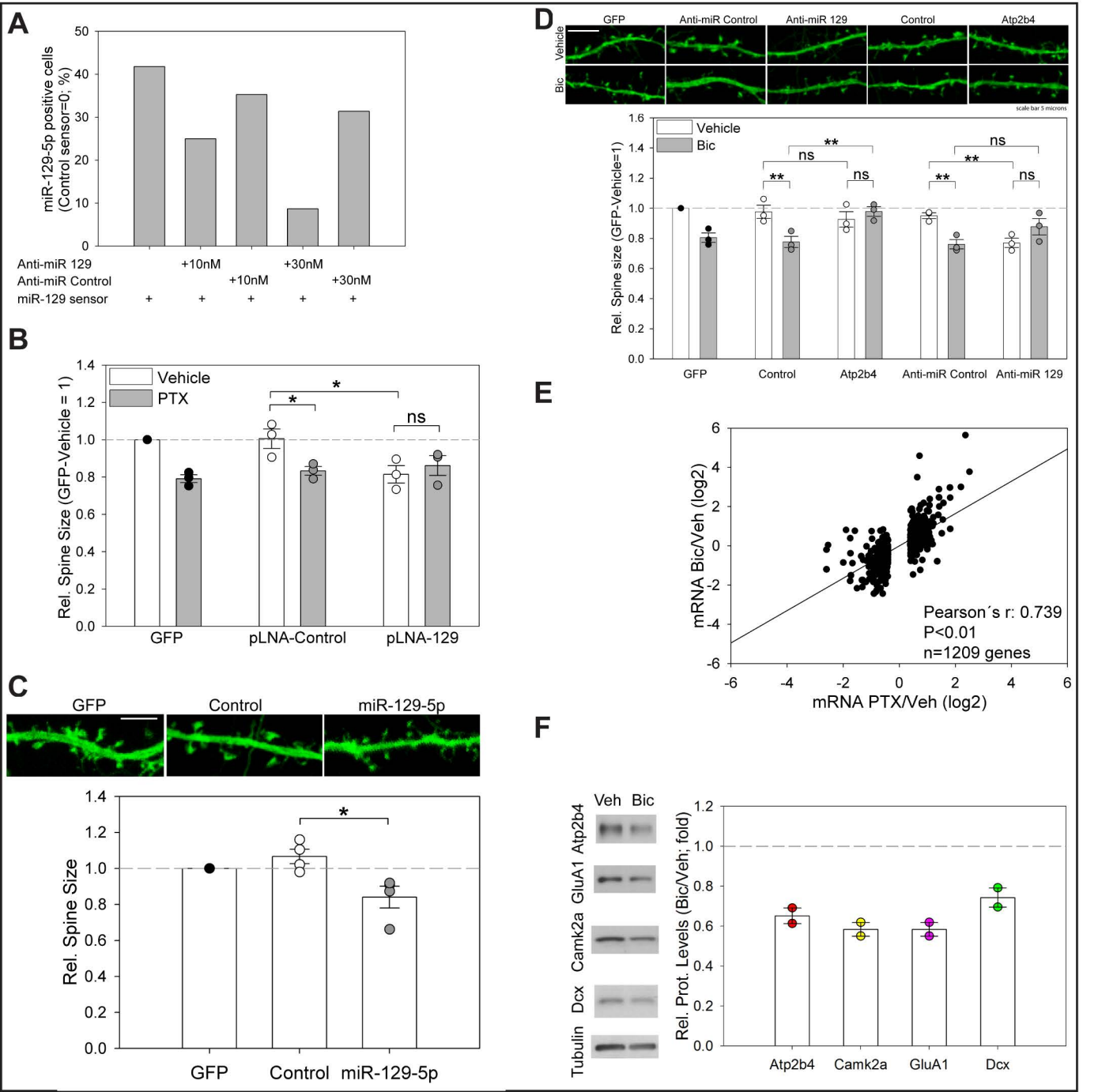

Appendix figure S2

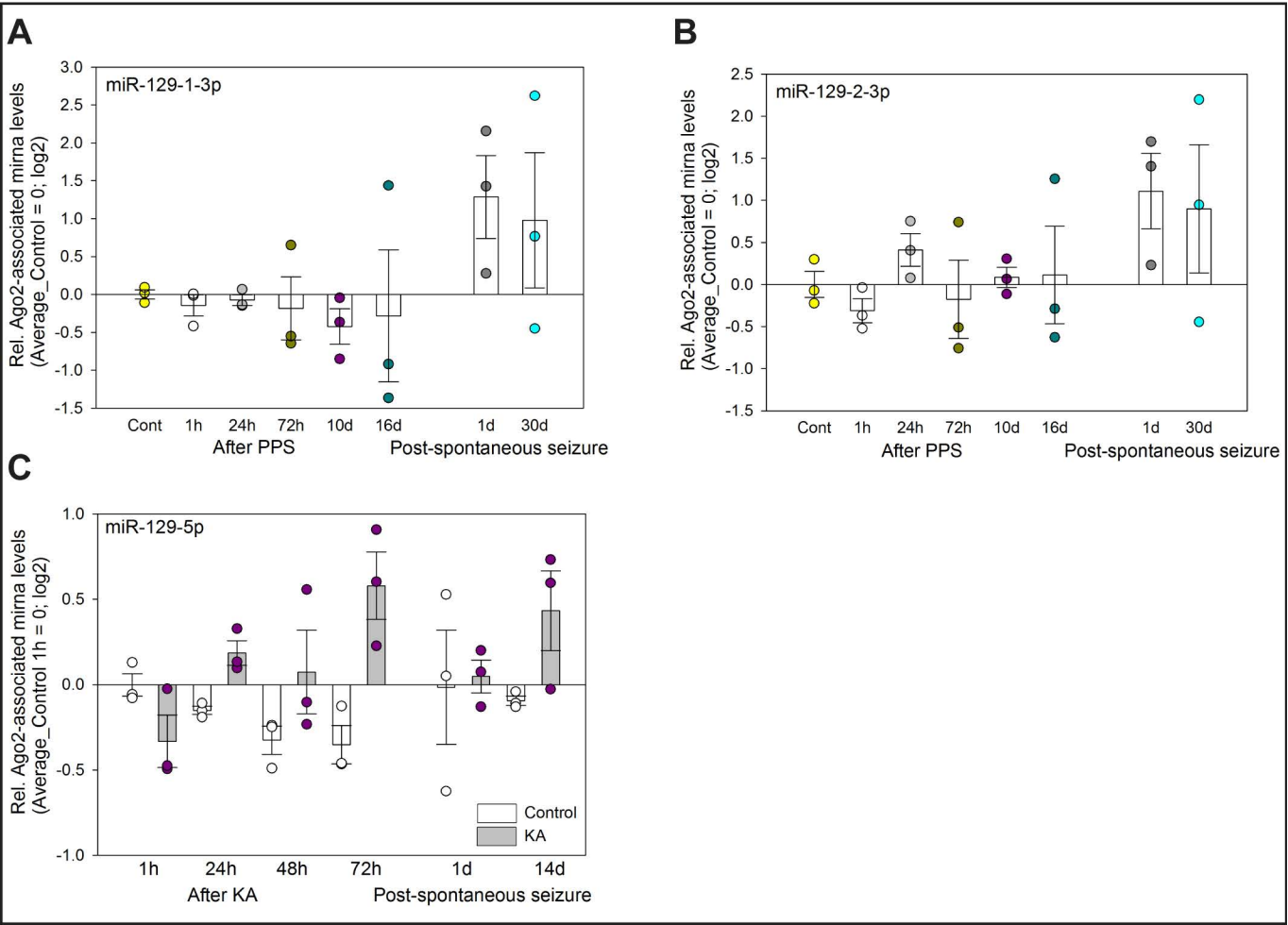

Appendix figure S3

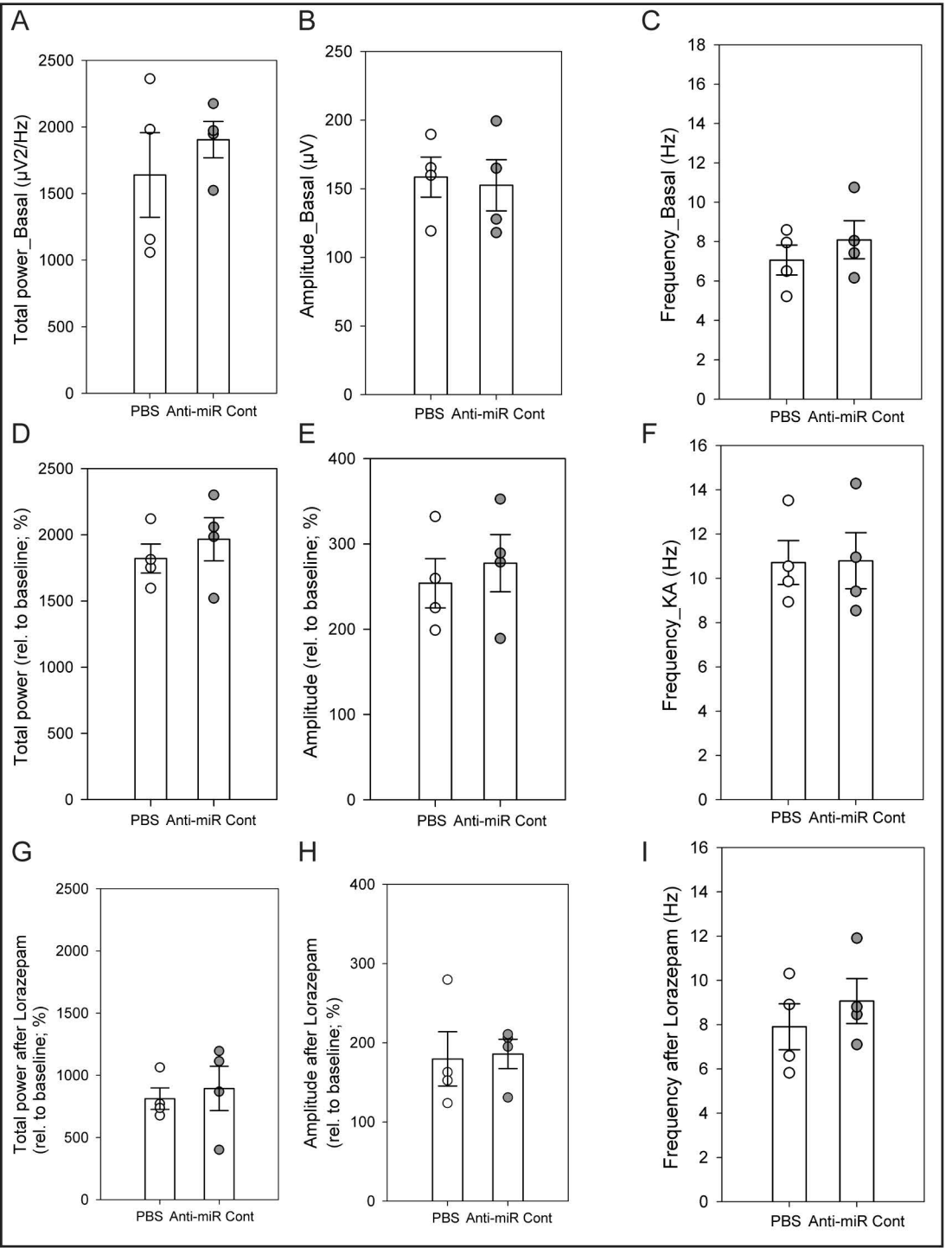

Appendix figure S4

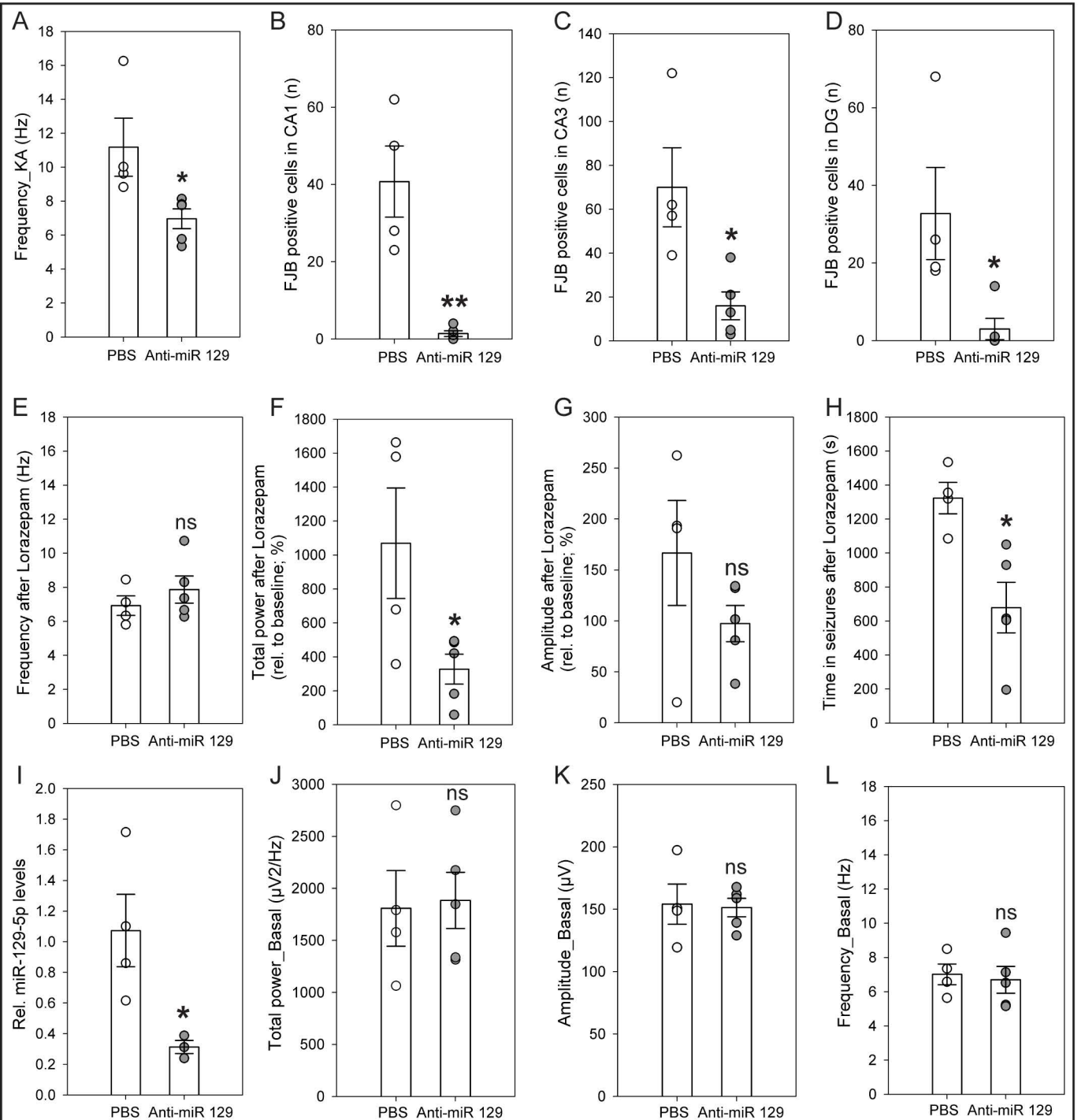

Appendix figure S5

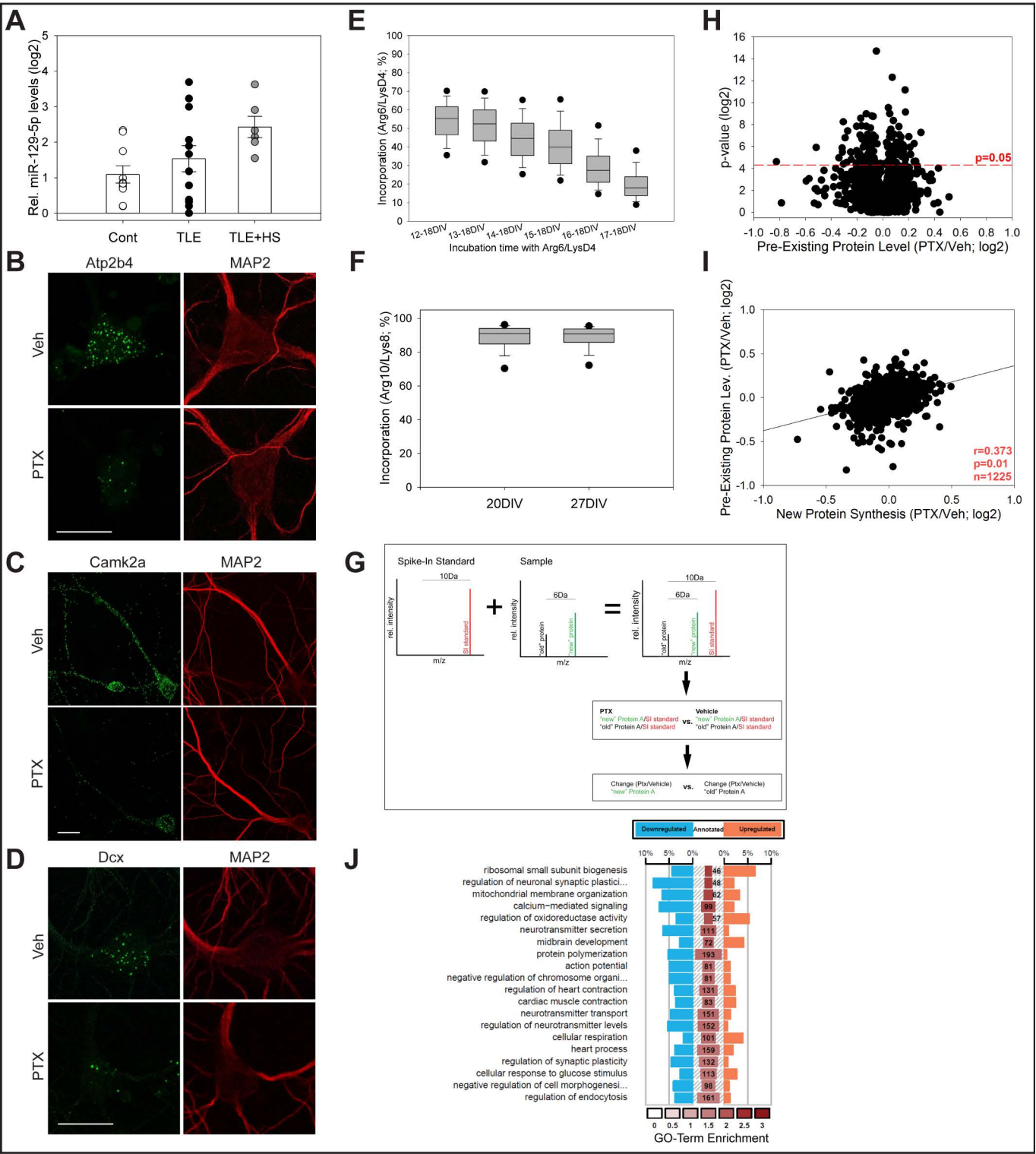

Appendix figure S6

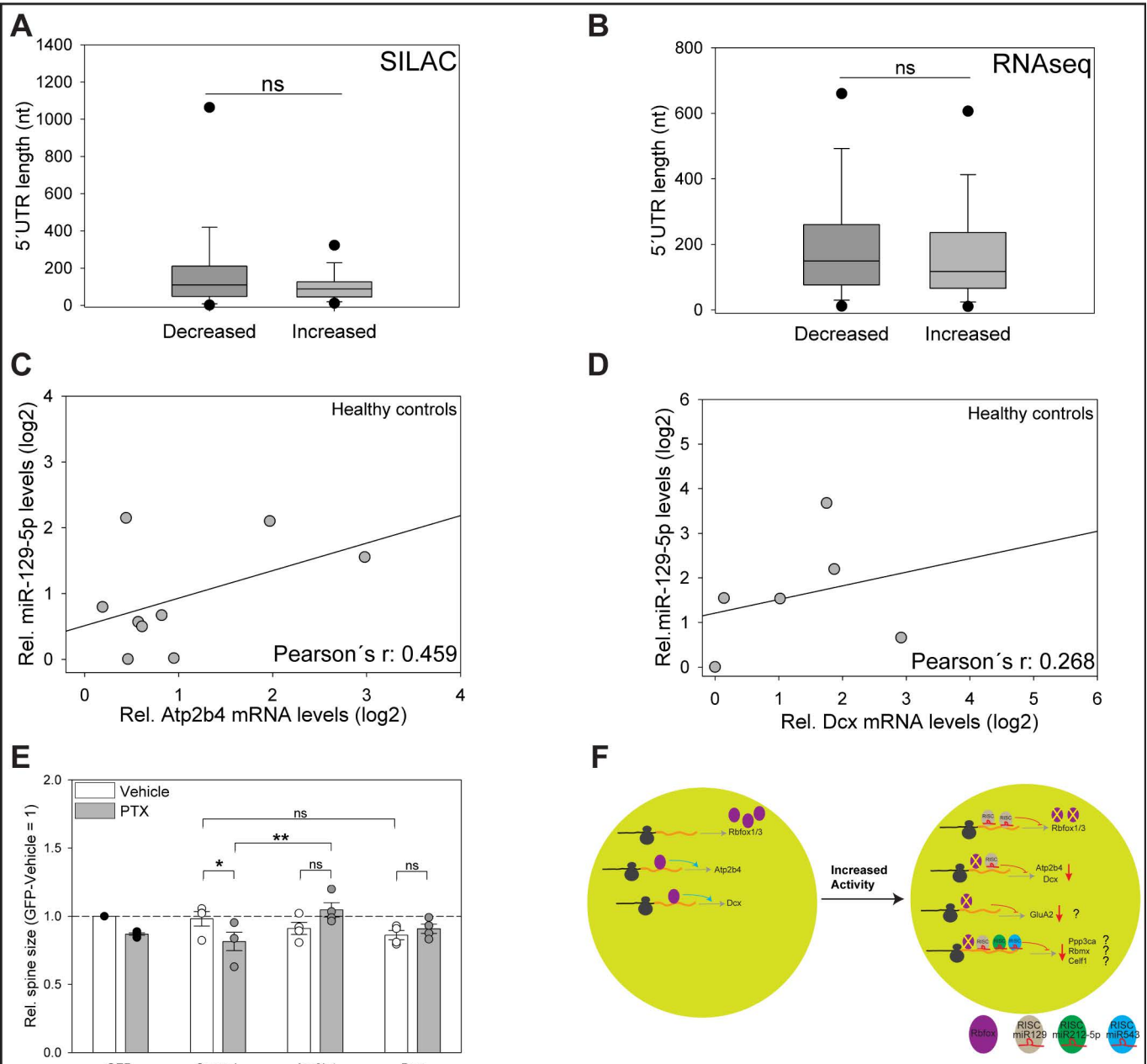

2. Appendix figure legends

Appendix figure S1

A) Validation of Anti-miR 129-5p specificity using a dual miRNA sensor assay. Values are presented as percent miR-129-5p positive cells after normalization to a control sensor lacking a miR-129-5p site.

B) Different presentation of the dataset shown in Fig. 2A. Dot-plot presentation with mean relative spine size (GFP-vehicle=1) +/- s.e.m. (n=3; GLM model, Estimated means of specific experimental conditions were compared by pairwise comparison in SPSS; details in Table EV12)

C) Upper panel: Representative confocal microscopy images of dendritic segments from GFP-, sh-Control-, control- or miR-129-5p-transfected hippocampal neurons (scale bar = 5 μm). Bottom panel: quantification of dendritic spine size from four independent experiments. Dot-plot presentation withe mean relative spine size (GFP=1) +/- s.e.m (n=4; 8 neurons, ~200 spines/neuron per experimental condition; independent two-sample t-test, 2-tailed, homoscedastic variance; details in Table EV12)

D) Upper panel: Representative confocal microscopy images of dendritic segments from GFP, Control Protein, Atp2b4, Anti-miR Control or Anti-miR 129 transfected hippocampal neurons (scale bar = 5μm). Bottom panel: quantification of dendritic spine size from three independent experiments. Dot-plot presentation with mean relative spine size (GFP=1) +/- s.e.m (n=3; 8 neurons, ~200 spines/neuron per experimental condition; GLM model, Estimated means of specific experimental conditions were compared by pairwise comparison in SPSS; details in Table EV12)

E) Comparison of transcriptome changes induced by 48 h PTX- or Bic stimulation of rat hippocampal neurons. Log2(PTX/control) is plotted vs. log2(Bic/control) for all differentially expressed genes (log2 fold changes ≥ 0.4 or ≤ -0.4) from one representative experiment (n=1209 genes, Pearson's r= 0.739; $P<0.01$). Individual values for all differentially expressed genes are listed in Table EV11.

F) Left: Representative Western blot for Atp2b4, Camk2a, GluA1 and Dcx using lysates from hippocampal neurons treated with either vehicle (Veh) or bicuculline (Bic; 20μM) for 48 h. Tubulin was used as a loading control. Right: Quantification of 2 independent experiments. Data are presented as a ratio Bic/Veh in a dot-plot with mean +/- s.e.m.

Appendix figure S2

A, B) qPCR analysis of miR-129-1-3p and miR-129-2-3p form samples presented in Fig 3A, MiR-129-1-3p (FDR=0.322) or miR-129-2-3p (FDR=0.349). C) KA epilepsy model. qPCR analysis of miR-129-5p was analyzed like in Fig 3A (FDR=0. 0242). Dot-plot presentation with mean +/- s.e.m (n = 3 mice per group).

Appendix figure S3

Additional EEG parameters of PBS and Anti-miR control injected mice.

A-C) Graphs show Total power (A), Amplitude (B) and Frequency (C) 24 h after injection with Anti-miR Control or PBS. Data are presented as dot-plot graphs with mean +/- s.e.m. (n = 4 mice per group; no difference was observed).

D-F) Graphs show EEG total power (D), amplitude (E) depicting % of increase from each animal's own baseline data, and frequency (F) during 40 min of observation after KA-induced status epilepticus in mice pretreated (24h) with PBS or Anti-miR Control. Dot-plot presentation with mean +/- s.e.m (n = 4 mice per group; no difference was observed).

G-I) Graphs show total EEG power (G) and Amplitude (H), depicting % of increase from each animal's own baseline data, and Frequency in Hz (I) during 1h of observation after lorazepam injection in mice pretreated (24h) with Anti-miR Control or PBS (n = 4 mice per group; no difference was observed).

Appendix figure S4

Additional EEG parameters of PBS and Anti-miR 129 injected mice.

A) Graph show Frequency (Hz) after KA treatment (A) in mice 24 h after injection with Anti-miR129 or PBS (n = 4–5 mice per group; independent two-sample t-test, 2-tailed, homoscedastic variance; *P < 0.05).

B-D) Graphs from CA1 (B), CA3 (C) and DG (D) of mice 24 h after status epilepticus in mice treated beforehand with PBS or Anti-miR 129 showing FJB counts. Quantification was performed as described in Fig. 6I (n = 4–5 mice per group; independent two-sample t-test, 2-tailed, homoscedastic variance; *P < 0.05; **P < 0.01).

E-H) Graphs show Frequency in Hz (E), total EEG power (D) and Amplitude (G), depicting % of increase from each animal's own baseline data, and time spent in seizures (H) during 1h of observation after lorazepam injection in mice pretreated (24h) with Anti-miR129 or PBS (n = 4–5 mice per group; independent two-sample t-test, 2-tailed, homoscedastic variance; *P < 0.05).

I) qPCR analysis of miR-129-5p levels from hippocampi of mice injected with PBS and Anti-miR 129-5p (n= 3–4 mice per group; independent two-sample t-test, 2-tailed, homoscedastic variance; *P < 0.05).

J-L) Graphs show Total power (J), Amplitude (K) and Frequency (L) before application of KA. Data are presented in a dot-plot with mean +/- s.e.m. (n = 4–5 mice per group; independent two-sample t-test, 2-tailed, homoscedastic variance; ns).

Appendix figure S5

A) qPCR analysis of miR-129-5p in the hippocampus of temporal lobe epilepsy patients with (TLE+HS; n=6) or without (TLE; n=12) documented hippocampal sclerosis (HS), as well as healthy controls (Cont; n=10). Data are presented as dot-plot graphs with mean +/- s.e.m.

B-D) Representative confocal microscopy images from FISH of PTX- or EtOH-treated hippocampal neurons using probes specific for Atp2b4 (B), Camk2a (C) or Dcx (D). MAP2 immunostaining was used to visualize dendrites. Scale bar represents 20 μm.

E) Incorporation of stable isotope amino acids in developing hippocampal neurons (12-18 DIV). Starting at 12 DIV, neurons were fed with Arg6/LysD4 (200uM/400uM) + Pro (1.72mM) for 1-6 days. Data are presented as box plots.

F) Development of spike-in standard. FUDR -treated HC were grown in neurobasal medium supplied with Arg10/Lys8 (200/400μM) and Pro (1.72mM) for 20 or 27 DIV. Data are presented as box plots.

G) A combination of spike-in standard and pulse labeling allows distinguishing pre-existing ("old") from newly synthesized ("new") proteins after PTX treatment.

H) Volcano plot showing average changes in pre-existing protein levels (PTX/Veh; log2) vs. p-value (log2) (n=3; 1225 proteins; independent one-sample t-test, 2-tailed, heteroscedastic variance). Proteins with P<0.05 were considered as differentially synthesized (total of 135 proteins, 72↓, 63↑).

I) Low correlation between changes (PTX/Veh; log2) in new and pre-existing protein levels (Pearson correlation coefficients; n=1225, r=0.373, P<0.001). J) Results from GO term analysis taking into account 182 differentially synthesized proteins (Fig 4D) based on pSILAC.

Appendix figure S6

A) Box plot representation of the 5´UTR length of gene sets used in Fig. 4D (Mann Whitney U test; ns: not significant).

B) Box plot representation of the 5´UTR length of gene sets used in Fig. 4A (Mann Whitney U test; ns: not significant).

C,D) Relation between miR-129-5p and Atp2b4 (C) or Dcx (D) expression levels in the hippocampus of human healthy controls. Data are represented as rel. RNA or miRNA levels (Atp2b4: n=9, Pearson's r= 0.459; P=0.214; Dcx: n=6, Pearson's r= 0.268; P=0.607).

E) Different representation of dataset shown in Fig. 6A. Dot-plot presentation with mean relative spine size (GFP-vehicle=1) +/- s.e.m. (n=4; GLM model, Estimated means of specific experimental conditions were compared by pairwise comparison in SPSS; details in Table EV12)

F) Model for the miR-129-5p/Rbfox crosstalk during synaptic downscaling. In low activity conditions (left cell), high levels of Rbfox proteins promote the expression of important synaptic genes (Atp2b4, Dcx), thereby maintaining synaptic strength. In response to chronic increases in neuronal activity (e.g. caused by 48h PTX treatment; right cell), upregulation of miR-129-5p induces a downregulation of synaptic genes containing miR-129-5p binding sites. At the same time, Rbfox proteins are repressed by direct interaction with miR-129-5p, potentially contributing to a further suppression of synaptic Rbfox targets (that do or do not contain miR-129-5p binding sites, such as GluA2). In addition, miR-129-5p independent suppression of a subset of synaptic genes (e.g. Ppp3ca, Celf1) might be achieved by other PTX-responsive miRNAs, such as miR-212 or miR-543). Interactions that were not experimentally tested in this study are labeled with a question mark.

3. Appendix Methods

Animal experiments

Procedures in mice were approved by the Research Ethics Committee of the Royal College of Surgeons in Ireland (REC-842), under license from the Health Products Regulatory Authority (AE19127/001), Dublin, Ireland. Procedures in rats were under authorization of Philipps University (Marburg, Germany) bioethics committee and approved by the local regulation authority (Regierungspräsidium Gieβen). Male adult C57BL/6JJ mice (20-25 g; Harlan, UK), and male Sprague-Dawley rats (300–400 g; Harlan-Winkelmann, Borchen, Germany) were used in all studies. Animals were housed in on-site barrier-controlled facilities having a 12 h light-dark cycle with ad libitum access to food and water.

Perforant pathway stimulation paradigms

Bipolar stainless-steel stimulating electrodes consisting of 2 stainless steel electrodes twisted together (diameter 0.125 mm, Plastics One, Roanoke, VA, USA) were placed bilaterally in the angular bundles of the perforant pathway (4.5 mm lateral from the sagittal suture and immediately rostral to the lambdoid suture). Unipolar recording electrodes (diameter 0.25 mm, Plastics One, Roanoke, VA, USA) were lowered into the brain bilaterally (2 mm lateral from the midline, 3 mm caudal to bregma). Final dorsoventral tip locations in the granule cell layer were reached by optimizing the potentials evoked by perforant pathway stimulation. Three screws were applied to the skull. For wireless long-term EEG recording, an EEG transmitter (Open Source Instruments, Watertown, MA, USA) was implanted subcutaneously and connected to the left dentate gyrus recording electrode and to a skull screw. A layer of dental acrylic cement attached the electrodes to the screws and skull. Plastic connectors (Plastics One, Roanoke, VA, USA) were fitted to the electrodes and then embedded in acrylic cement to form a mechanically stable cap. All stimulation protocols in Sprague–Dawley rats utilized a paradigm developed by 1. We used a Grass S88 stimulator in conjunction with a stimulus isolation unit (Grass Instruments, West Warwick, RI, USA). Thirty minutes of perforant pathway stimulation (PPS) on two consecutive days were followed by eight hours of PPS on day 3. This stimulation protocol leads to development of mesial temporal lobe epilepsy with classical hippocampal sclerosis (mTLE-HS). Stimulation consisted of continuous, bilateral 2 Hz paired-pulse stimuli with a 40-ms interpulse interval plus a 10-second train of 20 Hz single-pulse stimuli delivered once per minute. All pulses (0.1 ms duration) were delivered at 15 V. In case of status epilepticus or ongoing seizures after the 30

min PPS on days 1 and 2, epileptiform activity was terminated by short isoflurane anesthesia. Eight-hour stimulation on the third day did not cause convulsive SE or epileptiform electrographic activity that outlasted the stimulation.

Ago2IP and small RNA seq

Small RNA sequencing libraries were prepared from the purified RNA using the TruSeq Small RNA Sample Prep Kit (Illumina). To accommodate the low amount of RNA after IP, all kit reagents were reduced by half, and the PCR step was done using 15 cycles. The quality of the produced cDNA libraries was validated with the 2100 Bioanalyzer High Sensitivity DNA chip (Agilent) and the concentration was quantified using KAPA Library Quantification Kit (KAPA biosystems). The libraries were pooled as required and 50 bp single end sequencing was performed on the Illumina NextSeq500 (Sequencing by Exiqon).
FastX toolkit was used to quality 3' trim (quality cut-off 30) and filter (quality score of 30 on minimum 80% of bases) the raw sequencing data. Adaptor sequence was removed using cutadapt. Filtered sequencing reads were mapped to mature rat miRNA sequences from miRBase version 21 using Bowtie, allowing zero mismatches. Unmapped reads were 3'end trimmed, removing up to three A or T nucleotides, to account for nun-templated nucleotide addition of miRNAs, and the 3'end trimmed reads were mapped to mature rat miRNA sequences again. The resulting rat miRNA expression profile was normalized to reads per million mapping reads (RPM).

Focal-onset status epilepticus in mice

These cannulas were placed on the dura mater with the following coordinates from bregma: AP= +0.3 mm, L= +0.9 mm; and AP= -0,95 mm, L= +2.85; for i.c.v and i.a., respectively. After recovery from surgery, mice randomly injected (i.c.v.) with an 0.5 nmol/2 µl Anti-miR129, negative Anti-miR (Anti-miR Control) or PBS. Twenty-four hours later mice were connected to the lead socket of a swivel commutator, which was connected to an EEG (Grass TwiN digital EEG). A baseline recording was obtained for 10 min. Next, mice underwent status epilepticus induced by unilateral microinjection of kainic acid (KA; Sigma-Aldrich; 0.3 µg/0.2 µl) into the basolateral amygdala nucleus. Lorazepam (8 mg/kg, i.p.) was administered 40 min after kainic acid to reduce morbidity and mortality. Mice were followed up to 60 min after lorazepam administration for the appearance of seizures, by electrographic and behavioural methods. After the observation period, mice were deeply anesthetized

(pentobarbital), transcardially perfused [phosphate-buffered saline (PBS)] and brains removed for histological assessment.

EEG and behavior analysis

Seizures were defined as high-amplitude (> 2 x baseline) high-frequency (> 5 Hz) polyspike discharges lasting ≥10 seconds. From the EEG recordings we calculated total power, amplitude, frequency and total time spent in seizures. EEG total power and amplitude were plotted as percentage of baseline recording (each animal's EEG power or amplitude post seizure compared to its own baseline EEG). EEG recordings were separated into the 40 minutes period after intraamygdala KA injection up to the time of anticonvulsant administration and a second epoch covering a period of 1h after anticonvulsant.

Histopathology

Fresh-frozen coronal brain tissue sections (20 μm) were post-fixed in formalin, treated with 0.006% potassium permanganate solution, rinsed and transferred to FJB solution (0.001% in 0.1% acetic acid) (Chemicon). After staining, sections were rinsed again, dried, cleared and mounted in DPX (Sigma-Aldrich). Sections were imaged using a LEICA DM4000B epifluorescence microscope with LEICA DFC 310FX camera (20x objective). Fluorescence images were converted to grayscale and inverted such that degenerating neurons appeared black on a light grey background. Semi-quantification of damaged cells was performed at hippocampus for the CA1, CA3 and DG subfields. Counts were the average of two adjacent sections assessed by an observer masked to experimental group/condition.

DNA constructs

The vector shRNA-Control (Fiore et al, 2009) and shRNA-Rbfox1 (Hu et al, 2013) were previously described. CREB-VP16m has been provided by M.E. Greenberg (Harvard Medical School, Boston, USA) and was used as negative control in overexpression experiments. Egfp-hPMCA4b (Chicka & Strehler, 2003) was acquired from Addgene. The rat Dcx CDS was PCR amplified from neuronal enriched hippocampal cells (HC) cDNA and cloned into Egfp-C1 vector to obtain Egfp-C1-Dcx. Rat Camk2a 3´UTR was a kind gift from J.D. Richter. Camk2a 3´UTR was cloned into pGL4.13 vector to obtain pGL4.13-Camk2a 3´UTR. Fragments of Atp2b4 (XM_008769446.1: 5091 – 6361) and Dcx (NM_053379.3: 1313 – 2614) 3´UTRs were PCR amplified from neuronal enriched HC cDNA and cloned into pGL4.13 vector to obtain pGl4.13-Atp2b4 3´UTR and pGl4.13–Dcx 3´UTR 1st. Mutants

of conserved miR-129-5 binding sites were produced by site directed mutagenesis using Pfu Plus! DNA Polymerase (Roboklon) according to manufacturer instructions. Control sensor-pTracer-dsRed-GFP was described previously (Fiore et al, 2009). pTracer-dsRed-129sensor was constructed by cloning a oligonucleotide bearing two perfect miR-129 binding sites downstream of the dsRed coding sequence of pTracer-dsRed.

Cell culture, transfection and stimulation

Neuronal transfections were performed with Lipofectamine 2000 (Invitrogen) as described earlier (Valluy et al, 2015). For stimulation, 18DIV neurons were treated either with Picrotoxin (PTX; 100 µM final concentration, Sigma), bicuculline (Bic; 20 µM final concentration, Sigma) or solvent (ethanol absolute) for the indicated times. Cells were transfected with respective Anti-miRs (pLNAs, Exiqon). For spine assays HC were fixed at 20DIV for 15min in 4% paraformaldehyde/4% sucrose as described earlier(Fiore et al, 2014).

Image analysis

Images were taken with a confocal laser scanning microscope (Zeiss LSM 5 or Leica SP5) using a 63× objective at a resolution of 1,024 × 1,024 pixel corresponding to an image size of 144.72 × 144.72 µm (Leica SP5) or 142.86 × 142.86 µm (Zeiss LSM 5), the pinhole was set to 1 AU and the interval to 0.4 µm for z-stacks. For spine analysis, high-resolution z-stack images of GFP-positive neurons displaying pyramidal morphology were taken. Spine volumes were subsequently analyzed with the ImageJ software as previously described (Schratt et al, 2006). For each independent experiment on average 8-9 neurons per condition were analyzed.

Single molecule fluorescence in situ hybridization (smFISH)

The protease treatment step was omitted in order to maintain dendritic integrity. After completion of the FISH protocol, cells were processed for immunostaining, using an anti-MAP2 antibody (Sigma M9942; 1:1,000) in GDB buffer (0.02% gelatin–0.5% Triton X-100–PBS). Images were acquired on a Leica SP5 laser-scanning confocal microscope. For z-stack images of whole cells, 12 consecutive optical sections were taken at a 0.4 µm interval with a resolution of 1024x1024 pixels using a 63x objective and a digital zoom factor of 2.5. For images of cell bodies, 15 consecutive optical sections were taken at a 0.4 µm interval with a resolution of 512x512 pixels using a 63x objective and a digital zoom factor of 5. For all pictures, the pinhole was set to 1 AU. Laser settings were kept constant between experimental

conditions. Maximum intensity projections of the z-stacks were used for signal quantification, which was conducted in a blinded manner. The average fluorescence intensity was measured with ImageJ, using the MAP2 immunostaining as mask to define cell bodies and dendrites.

Preparation of protein extracts and western blot

Proteins were extracted by shaking for 20 min at 4°C on a horizontal shaker (Rotamax 120, Heidolph). Lysates were collected and centrifuged at maximum speed for 5 min at 4°C. The supernatant was kept and protein concentration was measured by Pierce™ BCA Protein Assay Kit (Thermo Scietific). Western blot was performed as described previously (Siegel et al, 2009). The following primary antibodies were used: rabbit polyclonal anti-tubulin (1:5,000, Cell Signaling), rabbit polyclonal anti-GluA1 (1:2,000, Thermo Scientific), mouse monoclonal anti-CamkIIa (1:2,000, Santa Cruz Biotechnology), mouse monoclonal Anti-Calcium Pump PMCA4 ATPase (1:2,000, Abcam), rabbit polyclonal anti-Dcx (1:12,500, Abcam), mouse monoclonal Anti-Fox1 (1:1,000, Millipore), rabbit polyclonal GAPDH (1:10,000, Cell Signaling), rabbit polyclonal 4E-BP1 (1:4,000, Cell Signaling), mouse monoclonal anti-β-Actin (1:10,000, Sigma), rabbit polyclonal anti-Synapsin 1 (1:4,000, Millipore), mouse monoclonal anti-NeuN, Clone60 (1:1,000, Millipore), mouse anti-Actin (clone AC-15 from Sigma-Aldrich, WB: 1:10,000), mouse anti-Ago2 (clone 2D4 from Wako, WB: 1:1000) Primary antibodies were recognized by horseradish peroxidase (HRP)-conjugated goat anti-rabbit antibody (1:20,000; 401,315; Calbiochem) and HRP-conjugated rabbit anti-mouse antibody (1:20,000; 402,335; Calbiochem). Secondary antibodies were detected by chemiluminescence with SuperSignal® West Pico Chemiluminescent Substrate (Thermo Scientific) and ECL Plus Western Blot Detection System (GE Healthcare).

Cross-linking assay for measuring cell surface expression of glutamate receptor subunits

Neuronal enriched cell cultures were incubated with the non membrane-permeable crosslinker BS^3 (Thermo Scientific), diluted in HBSS to a final concentration of 2mM, for 10min at 37°C by gentle shaking. To inactivate free BS^3 glycine was added (100mM final concentration) to the medium and incubated for an additional 10min. Cells were washed with cold HBSS and incubated with lysis buffer (25mN HEPES pH=7.4; 500mM NaCl; 2mM EDTA; 0.1% NP-40; Complete Protease Inhibitor Cocktail EDTA-free, Roche) as described before. Lysates were collected and centrifuged at maximum speed for 5min at 4°C.

Supernatant was kept and used for Western blot after the measurement of protein concentration (Pierce™ BCA Protein Assay Kit).

Electrophysiology

For recordings, cells were perfused at room temperature with a bath solution containing (in mM): 140 NaCl, 2.8 KCl, 2 CaCl2, 1 MgCl2, 10 glucose, and 10 HEPES (pH 7.3 with NaOH, 300-310 mOsm) with bicuculline (20 μM) and tetrodotoxin (1 μM). The pipette solution contained (in mM): 120 KGluconate, 15 KCl, 5 NaCl, 10 HEPES, 2 MgCl2, 10 EGTA, 4 MgATP, and 0.1 NaGTP (pH 7.3 with KOH, 290-300 mOsm). Patch pipettes had resistances of 4 - 5.5 MΩ. Neurons were held at −70 mV, data were acquired for total of 15min at a sampling rate of 20 kHz and filtered at 3 kHz. Series resistance was monitored every 5min and cells with uncompensated series resistance of <25 MΩ were accepted. mEPSCs were analyzed off-line with the Mini Analysis software (Synaptosoft Inc.) for 100-300 sec. from the last 5min of current recordings (threshold: −5 pA, filter: 2 kHz). Cells were recorded from 4 independent experiments.

Pulsed SILAC labeling of primary hippocampal neuronal cells

Analysis of arginine-6 and lysine-D4 incorporation rates

Briefly, lysates were precipitated for 1 h using 4 volumes of ice-cold acetone. The protein pellet was dissolved in 6M urea, 2M thiourea, 10mM HEPES, pH=8, reduced, alkylated, and subjected to digestion by the protease trypsin (Promega). Digested peptides were desalted, and concentrated by Stage Tips (Rappsilber et al, 2007). The LC-MS/MS analysis was performed with an Easy nano-HPLC system (Thermo Fisher Scientific) coupled to a nano-ESI source and a quadrupole Orbitrap mass spectrometer (QExactive, Thermo Fisher Scientific). Acquisition of MS spectra in a mass range of 350–1650 *m*/*z* was done using an AGC target of 3E6 at a resolution of 70,000 (200 *m*/*z*). The instrument worked in a data-dependent mode, isolation of the ten most intense peaks for HCD fragmentation (25 collision energy) in a 100–1650 *m*/*z* mass range. The AGC target was set to 5E5 combined with a resolution of 35,000 at 200 *m*/*z*, while a maximum injection time of 60 ms was used. Raw data were analyzed with the MaxQuant version 1.3.0.5 using a Fasta rat database (2012).

PTX experiment

Gels were stained with colloidal Blue Staining Kit (Invitrogen). Each gel lane (representing one sample each) was separated into 11 gel pieces and proteins were subjected to in gel digestion using the protease trypsin as described in (Shevchenko et al, 2006). After stage Tip

purification (Rappsilber et al, 2007) samples were analyzed by LC-MS/MS using an LTQ-Orbitrap Velos instrument (Konzer et al, 2013). Raw data were analyzed by 1.3.7.4 Maxquant. Newly synthesized proteins and pre-existing protein level were calculated as described in suppl. Fig.1C. Accuracy of mixing (sample mixed with neuronal spike-in standard in 1:1 ratio) was checked. If mixing was correct then: M/L (Arg6/LysD4 vs Arg/Lys) + H/L (Arg10/Lys8 vs Arg/Lys) = 1. If not calculations were corrected for this error. All experiments were performed in biological triplicates. We identified and quantified 1225 different proteins. To test if changes in new protein synthesis for specific genes were reproducible we used one sample t-test (2-tailed, heteroscedastic). Proteins with p-value < 0.05 were considered as differentially expressed (n=182; increased (n=85), decreased (n=97)).

Quantitative real-time PCR

For *in vivo* experiments with Anti-miR 129 application, 250 ng of RNA was reverse transcribed using stem-loop specific primers for mmu-miR-129 (Applied Biosystems) and real-time quantitative PCR was carried out on a 7900HT Fast Realtime System (Applied Biosystems) using TaqMan miRNA assays. Expression of RNU19 was used for normalization. A relative fold change in expression of miR-129 was determined using the ΔΔCT method (Jimenez-Mateos et al, 2012). Specific primers were purchased from Sigma (RNU19 and miR-129). Data were normalised to RNU19 and relative miRNA expression levels were quantified using the ΔΔCT method.

Small RNA seq

In brief, 6 small RNA libraries (3 control and 3 ptx) representing 3 biological replicates were prepared using NEBNext® Multiplex Small RNA Library Prep Set for Illumina® (Set 1) kit (New England BioLabs) as per manufacturer's instructions. Multiplexed small RNA libraries were sequenced for 50 cycles in a single lane of one Illumina HiSeq2000 flow cell. Raw sequencing reads were trimmed from 3' adapter (AGATCGGAAGAGCACACGTCT) and filtered according to quality using "percent = 90 and cut-off = 30" parameters of Fastx-Toolkit for fastq data on a Galaxy, a web-based genome analysis tool ((Goecks et al, 2010); https://usegalaxy.org/) reads that contained only adapter sequence or those that initially (before trimming) did not contain adapter sequence, as well as reads shorter than 15 nucleotides were discarded. The remaining reads were mapped to the rat mature miRNAs (miRBase v19) using default parameters (one mismatch, 3 nt in the 3′ or 5′-trimming variants,

3 nt in the 3′-addition variants) of Miraligner software (Pantano et al, 2010). Only miRNAs that are represented by at least 1 count per million (CPM) reads in three of the conditions were considered for further analysis. Differential expression analysis of miRNAs was performed using edgeR, a Bioconductor package (McCarthy et al, 2012; Robinson et al, 2010).

Bioinformatic analysis

Mapping

Raw reads were aligned to the rat genome version 5 (rn5) using STAR (Dobin et al, 2013) version 2.3.1z12 with the following parameters:

-limitOutSJoneRead 10

-outSAMstrandField intronMotif

-outSAMattributes All

-outFilterMultimapNmax 2

-outFilterMismatchNmax 5

-outFilterIntronMotifs RemoveNoncanonicalUnannotated

For differential gene expression, PCR duplicates were removed using MarkDuplicates from PicardTools (http://broadinstitute.github.io/picard) version 1.105 with the following parameters:

MAX_SEQUENCES_FOR_DISK_READ_ENDS_MAP=50000

MAX_FILE_HANDLES_FOR_READ_ENDS_MAP=8000

SORTING_COLLECTION_SIZE_RATIO=0.25

OPTICAL_DUPLICATE_PIXEL_DISTANCE=100

VALIDATION_STRINGENCY=STRICT

COMPRESSION_LEVEL=5

MAX_RECORDS_IN_RAM=500000

Differential gene expression

The differential gene expression was determined using the Cufflinks suite (Trapnell et al, 2010) version 2.2.1 . Gene abundance was calculated using cuffquant –library-type fr-firststrand and differential expression was estimated using cuffdiff. Both programs were used with the transcript reference downloaded from ENSEMBL (version 79) (Zerbino et al, 2015).

3'UTR length estimation

To have a greater coverage for the 3'UTR length estimation, all replicates of one condition were merged using samtools merge. The merged bam files were used as input for the isoform

structural change model (IsoSCM (Shenker et al, 2014)), which runs a de-novo transcript assembly and predicts different UTR isoforms.

java -Xmx2048m -jar ~/isoSCM/IsoSCM-2.0.7.jar assemble -s reverse_forward -t 3

The predicted isoforms were annotated using bedtools first with the gene model and second with stop-codon coordinates using intersectBed. The most expressed isoform was considered for all further analysis. Additionally, we only considered genes which were sufficiently covered to reliably estimate 3'UTR length (FPKM > 10). For transcripts that showed differential enrichment in CB or Process compartment, differences between 3'UTR length measured in Veh and Ptx condition (Veh/PTX) were calculated. Genes with high variability (difference>Average+1SD) were removed from the analysis. Afterwards, average 3'UTR length was calculated. In the case of evenly distributed transcripts the median of 4 measuements (CB Veh and PTX, Process Veh and PTX) was calculated. The length of exons in spliced UTRs was summed up to estimate the total UTR length excluding introns.

miRNA seeds and Rbfox motifs

To identify conserved miRNA targets, we subjected the previously downloaded multiple sequence alignments to the custom perl script (targetscan_60.pl), which we downloaded from TargetScanHuman version 6.2 (Lewis et al, 2005). Our set of miRNAs consisted of differentially expressed miRNAs at an FDR level of 0.05. All 8mer-1a and 7mer-m8 seeds occurring in rat were obtained and classified as poorly conserved (<= 3), conserved (4-9) and highly conserved (>= 10). The same analysis was performed for the Rbfox consensus motif ((U)GCAUG).

GO-Term enrichment

The GO-Term enrichment was performed using different Bioconductor packes in R such as biomaRt, topGO, and annotate. The plots were generated using CellPlot https://github.com/dieterich-lab/CellPlot.

CLIP Analysis

Publicly available CLIP-experiments (Ago (Chi et al, 2009), Mbnl2 (Charizanis et al, 2012), Mbnl1 (Wang et al, 2012), Ptbp2 (Licatalosi et al, 2012), Fus (Ishigaki et al, 2012), TDP43 (Polymenidou et al, 2011), nElavl (Ince-Dunn et al, 2012), Rbfox1/2/3 (Weyn-Vanhentenryck et al, 2014) were downloaded as bed files through the star database. Clip signals were annotated with mm9 features using python to map target sites to the corresponding genes and regions.

Code availability

Codes used in the bioinformatic analysis are https://github.com/dieterich-lab/rajman_et_al.

Real time PCR primers:

Camk2a:	FW (CGCCTGTACCAGCAGATCAAA)
	RW (CGGGTTGATGGTCAGCATCTT)
Dcx:	FW (GGAGTGCGCTACATTTACACT)
	RW (GTCTGAGGAACAGACATAGCTT)
Human Dcx:	described in (Santra et al, 2011)
Atp2b4:	FW (CAACAACTTGGTCCGGCACTT)
	RW (TGTAAGCTTGTACCACGGTCAT)
Human Atp2b4:	FW (CAATAACCTAGTACGGCACTT)
	RW (TATAAGCTTGTACCACAGTCAT)
Camk2b:	FW (GGAACACCAGGCTACCTGTCT)
	RW (CCACCAGCAGGATATACAGGAT)
U6:	described in (Valluy et al, 2015).

Statistics

Error bars represent s.e.m. P-values were calculated with independent Student's t-test (two-tailed). In the case of one-sample t-test we were comparing change vs 1 (not change). In this case we always assumed heteroscedasticity. In the case of two-sample t-test because of low number of biological replicates we could not reliably test for differences in variance between groups and therefore we assumed homoscedascity. When the data were not normally distributed, they were tested by nonparametric test - Mann Whitney U test. To characterize relation between different data points we used Pearson correlation analysis. In the case of RNAseq experiments correction for multiple comparisons was used. To compare the effect of two factors in electrophysiology we used General Linear Model by SPSS. Further, to see how the specific groups differ, we compared their estimated means by pairwise comparison (SPSS). Spine assays were analyzed by one-way ANOVA and specific groups were further compared by Bonferroni post hoc test (SPSS). When SPSS reported P=0.000 we present it as P<0.001.

Anti-miR 129 used in vivo experiments:

Sequence is: 5'-CCcAgAccGCaaAaA-3'. Capital letters are Locked Nucleic Acids (LNA) and small letters are DNA phosphorotioates.

References

Charizanis K, Lee KY, Batra R, Goodwin M, Zhang C, Yuan Y, Shiue L, Cline M, Scotti MM, Xia G, Kumar A, Ashizawa T, Clark HB, Kimura T, Takahashi MP, Fujimura H, Jinnai K, Yoshikawa H, Gomes-Pereira M, Gourdon G, et al. (2012) Muscleblind-like 2-mediated alternative splicing in the developing brain and dysregulation in myotonic dystrophy. *Neuron* **75:** 437-450

Chi SW, Zang JB, Mele A, Darnell RB (2009) Argonaute HITS-CLIP decodes microRNA-mRNA interaction maps. *Nature* **460:** 479-486

Chicka MC, Strehler EE (2003) Alternative splicing of the first intracellular loop of plasma membrane Ca2+-ATPase isoform 2 alters its membrane targeting. *J Biol Chem* **278:** 18464-18470

Dobin A, Davis C, Schlesinger F, Drenkow J, Zaleski C, Jha S, Batut P, Chaisson M, Gingeras T (2013) STAR: ultrafast universal RNA-seq aligner. *Bioinformatics* **29:** 15-21

Fiore R, Khudayberdiev S, Christensen M, Siegel G, Flavell SW, Kim TK, Greenberg ME, Schratt G (2009) Mef2-mediated transcription of the miR379-410 cluster regulates activity-dependent dendritogenesis by fine-tuning Pumilio2 protein levels. *EMBO J* **28:** 697-710

Fiore R, Rajman M, Schwale C, Bicker S, Antoniou A, Bruehl C, Draguhn A, Schratt G (2014) MiR-134-dependent regulation of Pumilio-2 is necessary for homeostatic synaptic depression. *EMBO J* **33:** 2231-2246

Goecks J, Nekrutenko A, Taylor J (2010) Galaxy: a comprehensive approach for supporting accessible, reproducible, and transparent computational research in the life sciences. *Genome Biol* **11:** R86

Hu J, Ho AL, Yuan L, Hu B, Hua S, Hwang SS, Zhang J, Hu T, Zheng H, Gan B, Wu G, Wang YA, Chin L, DePinho RA (2013) From the Cover: Neutralization of terminal differentiation in gliomagenesis. *Proc Natl Acad Sci U S A* **110:** 14520-14527

Ince-Dunn G, Okano HJ, Jensen KB, Park WY, Zhong R, Ule J, Mele A, Fak JJ, Yang C, Zhang C, Yoo J, Herre M, Okano H, Noebels JL, Darnell RB (2012) Neuronal Elav-like (Hu) proteins regulate RNA splicing and abundance to control glutamate levels and neuronal excitability. *Neuron* **75:** 1067-1080

Ishigaki S, Masuda A, Fujioka Y, Iguchi Y, Katsuno M, Shibata A, Urano F, Sobue G, Ohno K (2012) Position-dependent FUS-RNA interactions regulate alternative splicing events and transcriptions. *Sci Rep* **2:** 529

Jimenez-Mateos EM, Engel T, Merino-Serrais P, McKiernan RC, Tanaka K, Mouri G, Sano T, O'Tuathaigh C, Waddington JL, Prenter S, Delanty N, Farrell MA, O'Brien DF, Conroy RM, Stallings RL, DeFelipe J, Henshall DC (2012) Silencing microRNA-134 produces neuroprotective and prolonged seizure-suppressive effects. *Nat Med* **18:** 1087-1094

Konzer A, Ruhs A, Braun H, Jungblut B, Braun T, Kruger M (2013) Stable isotope labeling in zebrafish allows in vivo monitoring of cardiac morphogenesis. *Mol Cell Proteomics* **12:** 1502-1512

Lewis B, Burge C, Bartel D (2005) Conserved Seed Pairing, Often Flanked by Adenosines, Indicates that Thousands of Human Genes are MicroRNA Targets. *Cell* **120:** 15-20

Licatalosi DD, Yano M, Fak JJ, Mele A, Grabinski SE, Zhang C, Darnell RB (2012) Ptbp2 represses adult-specific splicing to regulate the generation of neuronal precursors in the embryonic brain. *Genes Dev* **26:** 1626-1642

McCarthy DJ, Chen Y, Smyth GK (2012) Differential expression analysis of multifactor RNA-Seq experiments with respect to biological variation. *Nucleic Acids Res* **40:** 4288-4297

Pantano L, Estivill X, Marti E (2010) SeqBuster, a bioinformatic tool for the processing and analysis of small RNAs datasets, reveals ubiquitous miRNA modifications in human embryonic cells. *Nucleic Acids Res* **38:** e34

Polymenidou M, Lagier-Tourenne C, Hutt KR, Huelga SC, Moran J, Liang TY, Ling SC, Sun E, Wancewicz E, Mazur C, Kordasiewicz H, Sedaghat Y, Donohue JP, Shiue L, Bennett CF, Yeo GW, Cleveland DW (2011) Long pre-mRNA depletion and RNA missplicing contribute to neuronal vulnerability from loss of TDP-43. *Nat Neurosci* **14:** 459-468

Rappsilber J, Mann M, Ishihama Y (2007) Protocol for micro-purification, enrichment, pre-fractionation and storage of peptides for proteomics using StageTips. *Nat Protoc* **2:** 1896-1906

Robinson MD, McCarthy DJ, Smyth GK (2010) edgeR: a Bioconductor package for differential expression analysis of digital gene expression data. *Bioinformatics* **26:** 139-140

Santra M, Santra S, Buller B, Santra K, Nallani A, Chopp M (2011) Effect of doublecortin on self-renewal and differentiation in brain tumor stem cells. *Cancer Sci* **102:** 1350-1357

Schratt GM, Tuebing F, Nigh EA, Kane CG, Sabatini ME, Kiebler M, Greenberg ME (2006) A brain-specific microRNA regulates dendritic spine development. *Nature* **439:** 283-289

Shenker S, Miura P, Sanfilippo P, Lai E (2014) IsoSCM: improved and alternative 3' UTR annotation using multiple change-point inference. *RNA* **21:** 14-27

Shevchenko A, Tomas H, Havlis J, Olsen JV, Mann M (2006) In-gel digestion for mass spectrometric characterization of proteins and proteomes. *Nat Protoc* **1:** 2856-2860

Siegel G, Obernosterer G, Fiore R, Oehmen M, Bicker S, Christensen M, Khudayberdiev S, Leuschner PF, Busch CJ, Kane C, Hubel K, Dekker F, Hedberg C, Rengarajan B, Drepper C, Waldmann H, Kauppinen S, Greenberg ME, Draguhn A, Rehmsmeier M, et al. (2009) A

functional screen implicates microRNA-138-dependent regulation of the depalmitoylation enzyme APT1 in dendritic spine morphogenesis. *Nat Cell Biol* **11:** 705-716

Trapnell C, Williams B, Pertea G, Mortazavi A, Kwan G, van Baren M, Salzberg S, Wold B, Pachter L (2010) Transcript assembly and quantification by RNA-Seq reveals unannotated transcripts and isoform switching during cell differentiation. *Nature Biotechnology* **28:** 511-515

Valluy J, Bicker S, Aksoy-Aksel A, Lackinger M, Sumer S, Fiore R, Wust T, Seffer D, Metge F, Dieterich C, Wohr M, Schwarting R, Schratt G (2015) A coding-independent function of an alternative Ube3a transcript during neuronal development. *Nat Neurosci* **18:** 666-673

Wang ET, Cody NA, Jog S, Biancolella M, Wang TT, Treacy DJ, Luo S, Schroth GP, Housman DE, Reddy S, Lecuyer E, Burge CB (2012) Transcriptome-wide regulation of pre-mRNA splicing and mRNA localization by muscleblind proteins. *Cell* **150:** 710-724

Weyn-Vanhentenryck SM, Mele A, Yan Q, Sun S, Farny N, Zhang Z, Xue C, Herre M, Silver PA, Zhang MQ, Krainer AR, Darnell RB, Zhang C (2014) HITS-CLIP and integrative modeling define the Rbfox splicing-regulatory network linked to brain development and autism. *Cell Rep* **6:** 1139-1152

Zerbino D, Wilder S, Johnson N, Juettemann T, Flicek P (2015) The Ensembl Regulatory Build. *Genome Biology* **16:** 56

4. Appendix results

SILAC strategy used to quantify changes at the level of new protein synthesis upon PTX

Due to the low metabolic activity of neurons, labeling had to be initiated already 3 days prior to PTX treatment to obtain sufficient label incorporation (~50%; Appendix Fig. 5E, Table EV5). Therefore, one could argue that the observed changes in protein levels in our pSILAC experiment are not caused by changes in mRNA translation, but rather by altered mRNA transcription and/or protein stability (Ibata et al, 2008; Seeburg et al, 2008). In order to distinguish changes in "pre-existing" from newly synthesized proteins, we further spiked in a standard lysate that was obtained by labeling an independent set of neurons for 20 days with Arg10/Lys8 (~90% incorporation, Appendix Fig. 5F, Table EV6). This enabled the simultaneous quantification of changes in both de novo synthesized and pre-existing proteins (Appendix Fig. 5G). We observed a low positive correlation ($r=0.373$, $P<0.01$, $n=1225$ proteins) between PTX-dependent changes occurring at the level of pre-existing or newly synthesized proteins, suggesting that our experimental approach is able to differentiate between protein degradation and protein synthesis (Appendix Fig. 5H,I).

References

Ibata K, Sun Q, Turrigiano GG (2008) Rapid synaptic scaling induced by changes in postsynaptic firing. *Neuron* **57:** 819-826

Seeburg DP, Feliu-Mojer M, Gaiottino J, Pak DT, Sheng M (2008) Critical role of CDK5 and Polo-like kinase 2 in homeostatic synaptic plasticity during elevated activity. *Neuron* **58:** 571-583